

P0906-090-Chnani

Macroscopic Model of Solid Oxide Fuel Cell Stack for Integrating in a Generator Simulation

**Moussa Chnani, Marie-Cécile Péra, Raynal Glises
and Jean-Marie Kauffmann**

Laboratoire de Recherche en Electronique, Electrotechnique et Systèmes (L2ES)
Unité mixte UFC – UTBM
Associée à l'INRETS
LRE-T31 UTBM
13 Rue Thierry Mieg, Bâtiment F
FR-90010 Belfort Cedex / France
Tel.: + 33-3-8458- 3625
Fax: 33-3-8458-3636
moussa.chnani@utbm.fr

Abstract

This paper presents a macroscopic model of solid oxide fuel cell (SOFC) with the aim to perform a simulation of the whole generator. Three sub-models have been developed to take into fluidic, thermal and electrical phenomena.

The fluidic sub-model is based on an equivalent circuit based on electrical analogy. Pressure drops in channels are modelled by resistances and the fluid accumulation in the volume is modelled by capacitor. Each electrode compartment (channel+electrode) is represented by two resistances and one capacitor. We have used this model to calculate the pressure at the catalytic sites and gas flows at fuel cell input and output.

The electrical response is based on the classical Nernst potential equation, activation, ohmic and concentration overvoltages.

The thermal modelling is based on a (2D) nodal network. Two aspects are studied in this article (conduction and the convection heat transfer).

Results have been validated on a 5 cell stack.

Introduction

The solid oxide fuel cell (SOFC) is a promising technology. It is highly efficient, tolerant to impurities so it is fuel flexible (methane or even gasoline and diesel), and it can provide internal reforming of hydrocarbon fuels, at least partially. The work presented in this paper is in the frame work of the European project FELICITAS which aims to increase efficiency and life time of FC systems for heavy duty transportation applications (marine, rail, truck). One of the topics is the study of the hybridization of a PEFC and a SOFC. The model proposed here addresses a macroscopic simulation of a SOFC stack. It aims to be included in the simulation of the SOFC and PEFC coupling.

Three sub-models have been developed to compute the fluidic, electrical and thermal responses inside the fuel-cell stack (temperature and chemical species dynamics are considered). The stack cells are not modelled individually: a single average cell is considered, the gas flows and the voltage are related to the number of cells.

The fluid modelling is based on electric fluid analogy. Pressure drops in channels are modelled by two resistances (R_1 for the inlet pressure drop of the stack and R_2 for the

outlet pressure drop). The fluid accumulation in the electrode compartment volume (channel and electrode) is modelled by a capacitor. We have used this model to calculate the pressure at the catalytic sites and gas flow at fuel cell input and output [1].

The electrical response is based on Nernst potential equation at equilibrium, ohmic, activation and concentration overvoltages.

The thermal conduction and convection phenomena are taken into account in each cell are modelled by nodal network. The modelling principle by nodal network consists in establishing a co-relation with an electrical network. The considered system is separated into isothermal elements of volume V_i with temperature T_i . Each element "i" has a heat capacity C_i applied to center i of V_i and possibly a heat power generation. The item "i" is called node of the system. To simplify the model, one node in the medium is selected in each volume (anode, cathode, electrolyte and interconnects).

The heat balance resulting from the first principle of thermodynamics is applied to the node "i". Steady state and transient state thermal behaviours are presented.

SOFC principles

The SOFC can be operated with reformat hydrogen mixed with CO. Nevertheless, in this paper, operation with pure hydrogen is considered. In this case, the operation principle is based on the following mechanism: oxygen is dissociated with O^{2-} in a cathode, and then the anion migrates through the ionic conducting electrolyte at high temperature and will combine with hydrogen, to form water and to release from the electrons (figure 1).

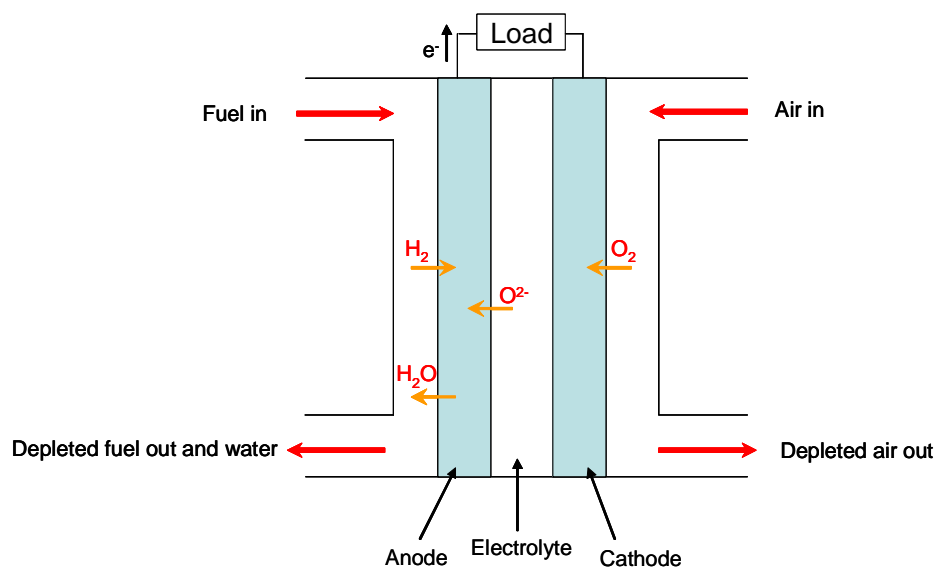
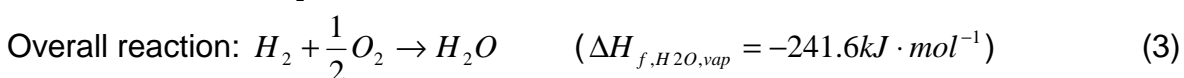


Figure 1 Principles of solid oxide fuel cell

Following reactions are considered:



The cell operates between 700°C and 850°C where ion ic conduction by oxygen ions takes place. So the thermal phenomena are very important.

R-design Stack: specifications and operation conditions

Experimental results have been provided by HTceramix company on their stacks. HTceramix produces its own unique stack design based on its SOFCConnex technology and HTc cells. The R-design stack uses an internal manifolding through feeding holes and is fuelled in a counter-flow configuration. ;

The stacks are operated with a nominal power density higher than $0.4\text{W}/\text{cm}^2$ at a temperature below 800°C . Electrical efficiencies of 40% have been commonly reached. The stacks can be fuelled with hydrogen, reformed hydrocarbons and synthesis gas mixtures, but the results provided in this article have been obtained with pure hydrogen. The stack R-design is composed of 5 repeating cells (figure 2).

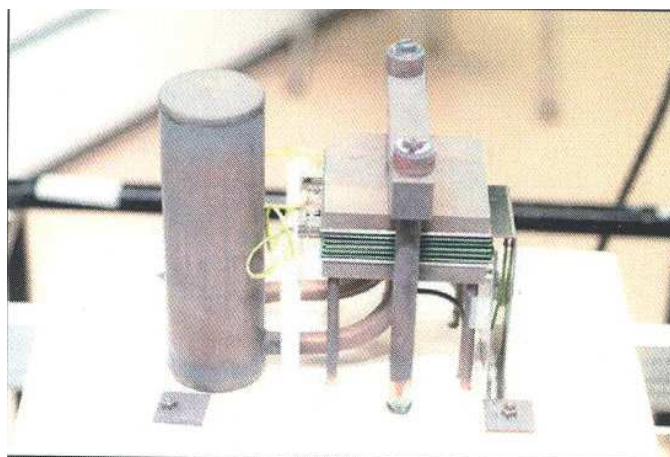


Figure 2 R-design stack developed by HTCermaix company

The following table illustrates the specifications and operation conditions:

Number of cells in stack	5	
Size of cells	80*80	mm×mm
Active area per cell	50	cm ²
Stack's dimensions	Depth	125.5 mm
	Length	132 mm
	Height	Cells*3 mm
	Weight	Cells*75 g
Minimum operating voltage per cell	0.6	V
Ideal operating voltage per cell	0.7	V
Ideal operating temperature	750	°C
Max. operating temperature	830	°C
Operating pressure	Atmospheric	
Fuel	Hydrogen or reformat	
Hydrogen volume flow rate per cell	200-400 (4-8 ml/min.cm ²)	
Oxidant flow rate ratio (lambda)	2-4	
Pressure drop on air side	20	mbar
Pressure drop on fuel side	10	mbar

Table 1 R-design stack, specifications and operation conditions

Macroscopic Model of SOFC

Model assumptions

The stack model will be based on the following assumptions:

- The stack is fed with hydrogen and air.
- The gases are ideal.
- The gas flowing in anode side and cathode side have the same direction.
- The channels (anode and cathode) have a fixed volume.
- The effect of radiation between gas and solid in the channels is neglected.

Fuel cell fluid modelling

The fluidic behaviour in anode and cathode side has been modelled using an electric fluid analogy [1]. In a formal approach, the flow is related to a current and the pressure is related to a voltage. It is considered that the pressure drop on air side and fuel side is linear with the air flow and fuel flow.

So, each electrode of volume V is modelled with an electric circuit (figure 3):

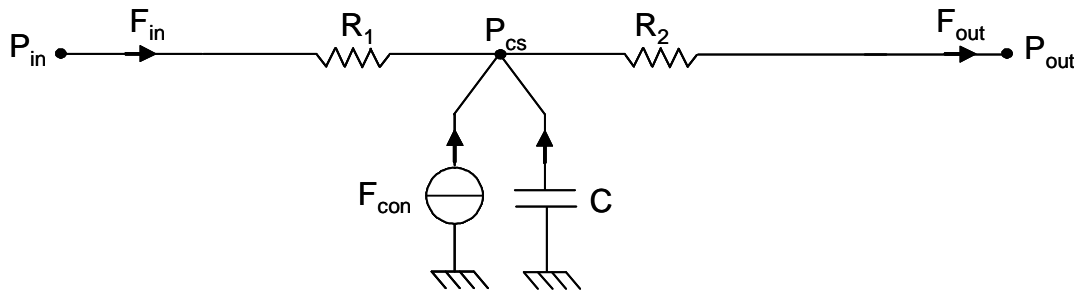


Figure 3 principle of fluidic modelling

Where:

P_{in} : electrode inlet pressure (mbar)

P_{out} : electrode outlet pressure (mbar)

F_{in} : inlet flow (mol/s)

F_{out} : outlet flow (mol/s)

F_{con} : consumed flow of each species in the electrode

R_1 : upstream fluidic resistance of the electrode

R_2 : downstream fluidic resistance of the electrode

C : fluidic capacity of the electrode

P_{cs} : pressure in the catalytic sites

Anode fluidic modelling

The stack is at atmospheric operating pressure, so the outlet partial pressure of hydrogen and water are given by equation 4:

$$p_{s(H_2)} + p_{s(H_2O)} = 1atm \quad (4)$$

Flows of each species:

$$F_{outH_2} = F_{inH_2} + F_{aH_2} + F_{conH_2} \quad (5)$$

$$F_{outH_2O} = F_{inH_2O} + F_{aH_2O} + F_{prH_2O} \quad (6)$$

Where:

F_{inH_2}, F_{outH_2} : Hydrogen Inlet and outlet flow.

F_{inH_2O}, F_{outH_2O} : Water inlet and outlet flow.

F_{aH_2}, F_{aH_2O} : Hydrogen flow and water flow in anodic fluid capacity.

F_{conH_2} : Hydrogen consumed flow in reaction (1).

F_{prH_2O} : Water produced flow in reaction (1).

The mole quantity of hydrogen in the chemical reaction is equal to the quantity of water produced:

$$F_{conH_2} = -F_{prH_2O} = -\frac{N_{cell} \times I}{2 \times F} \quad (7)$$

Where:

N_{cell} : Number of cells in stack

I : Stack current (A)

F : Faraday's constant

Every individual gas will be considered separately, and the perfect gas equation will be applied to it, hydrogen will be considered as an example [2] [3],

$$p_{H_2} \cdot V_A = n_{H_2} \cdot R \cdot T_A \quad (8)$$

Where, V_A is the volume of the anode, n_{H_2} is the hydrogen mole numbers in the anode channel; R is the universal gas constant and T_A is the absolute anode temperature.

$$\frac{n_{H_2}}{p_{H_2}} = \frac{V_A}{R \cdot T_A} \quad (9)$$

Thus, the hydrogen fluidic capacity is given by the following relation:

$$C_{H_2} = \frac{V_A}{R \cdot T_A} \quad (10)$$

Where:

p_{H_2} : Hydrogen partial pressure

T_A : Anode temperature

C_{H_2} : Fluidic capacity for hydrogen

Cathode fluidic modelling

The underlying equations make it possible to model the fluidic cathode side:

$$n_{air} = n_{O_2} + n_{N_2} \quad (11)$$

$$F_{outO_2} = F_{inO_2} + F_{cO_2} + F_{conO_2} \quad (12)$$

$$F_{outN_2} = F_{inN_2} \quad (13)$$

$$F_{conO_2} = -\frac{N_{cell} \times I}{4 \times F} \quad (14)$$

$$C_{O_2} = \frac{V_C}{R \cdot T_C} \quad (15)$$

Where:

n_{O_2} : Oxygen mole number

n_{N_2} : Nitrogen mole number

F_{inO_2}, F_{outO_2} : Oxygen Inlet and outlet flow.

F_{inN_2}, F_{outN_2} : Nitrogen inlet and outlet flow.

F_{cO_2} : Oxygen flow in cathodic fluid capacity.

F_{conO_2} : Oxygen consumed flow in reaction (1).

V_C, T_C : Cathode volume and temperature

Calculation of stack voltage

Applying Nernst's equation and Ohmic, activation, concentration overvoltages, the stack output voltage is represented by the following expression [2] [4] [5] [6] [7]:

$$V_{stack} = N_{cell} \cdot V_{cell} = N_{cell} \left\{ \underbrace{E^0 + \frac{RT}{2F} \left(\frac{P_{H_2} \cdot P_{O_2}^{0.5}}{P_{H_2O}} \right)}_{OCV} - r \times I - \eta_{act} - \eta_{con} \right\} \quad (16)$$

Where:

E^0 : Standard reversible cell potential [V]

T : Temperature of the stack [K].

P_{H_2}, P_{H_2O} : Partial pressure for hydrogen and water vapour at the electrolyte/anode interface [bar].

P_{O_2} : Partial pressure of oxygen at electrolyte/cathode interface [bar].

r : Ohmic resistance of one cell [Ω].

η_{act} : Activation overvoltage of one cell [V].

η_{con} : Concentration overvoltage of one cell [V].

Open circuit voltage

The OCV is given by equation 17.

$$OCV = E^0(T) + \frac{RT}{2F} \left(\frac{P_{H_2} \cdot P_{O_2}^{0.5}}{P_{H_2O}} \right) \quad (17)$$

The function $E^0(T)$ is empirical equation and is calculated from the comparison of the experimental OCV curve versus temperature measured on the stack (figure 4) and the theoretical OCV expression (equation 17).

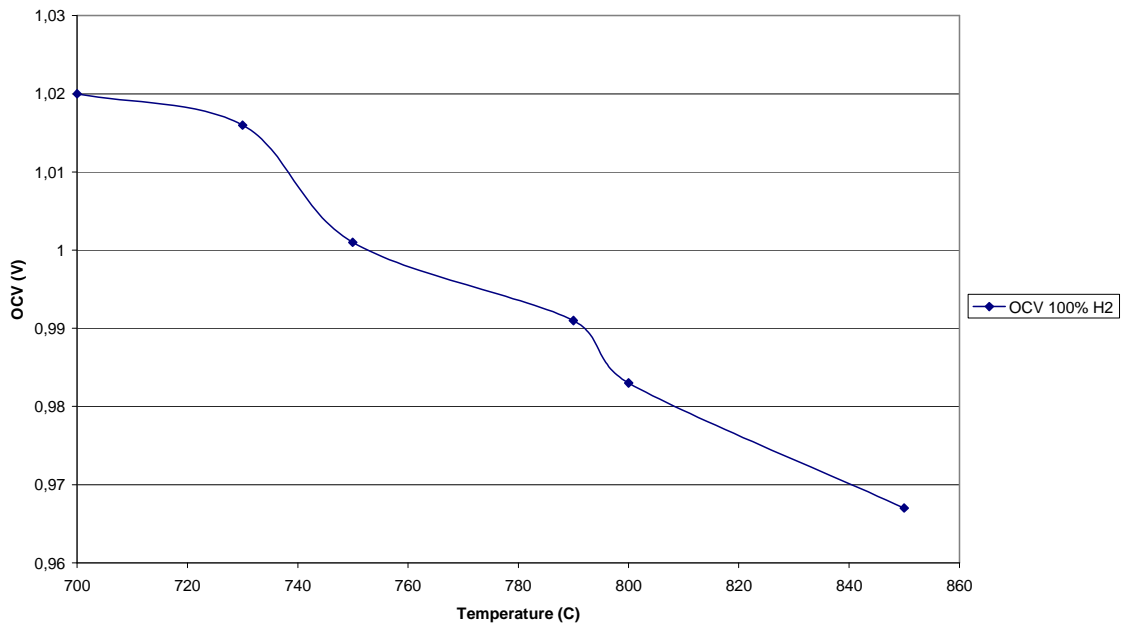


Figure 4 5-cell stack OCV variation with temperature related to one average cell

The variation of the OCV is given by the following expression

$$OCV = a_0 + a_1 \cdot T + a_2 \cdot T^2 + a_3 \cdot T^3 + a_4 \cdot T^4 + a_5 \cdot T^5 \quad (18)$$

The ohmic overvoltage is due to the flow of ions in the electrolyte and to the resistance to the flow of electrons through the electrode materials. Ohmic resistance is given by expression 19:

$$r = \frac{ASR}{A} \quad (19)$$

Where :

A : Active area [cm^2].

ASR : Area specific resistance [$\Omega \cdot cm^2$]

A special instrumentation was used for this stack in order to separate area specific resistance (ASR) contribution from each component.

The figure 5 shows the variation of the ASR with temperature

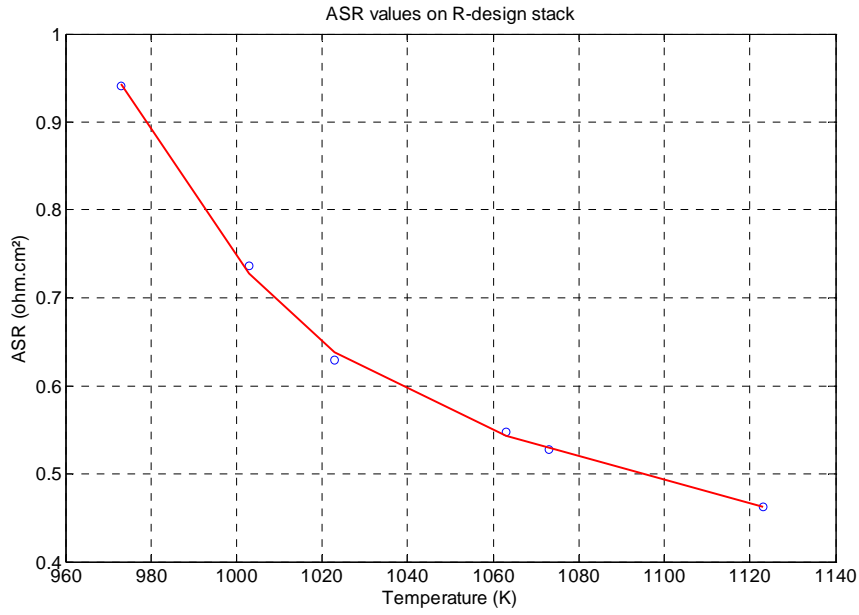


Figure 5 ASR variation with temperature related to one cell of the stack

The ASR function with temperature is interpolated by a polynome (equation 20):

$$ASR = b_0 + b_1 \cdot T + b_2 \cdot T^2 + b_3 \cdot T^3 \quad (20)$$

The numerical values are available in Table 2.

	<i>a</i>		<i>b</i>
1	-7.3500E004	1	265.0306
2	352.8520	2	-0.7281
3	-0.6772	3	6.6900E - 004
4	6.4941E - 004	4	-2.0523E - 007
5	-3.1121E - 007		
6	5.9621E - 011		

Table 2 Numerical values

Activation overvoltage

The activation overvoltage is directly related to the rates of electrochemical reactions [6] [8], the expression of the activation overvoltage is given by:

$$\eta_{act} = \frac{RT}{\alpha n F} \ln\left(\frac{i}{i_0}\right) \quad (21)$$

Where:

α : Electron transfer coefficient

n : Number of electron

i : Current density [A/cm²]

i_0 : Exchange current density [A/cm²]

We can write this overvoltage of an empirical equation:

$$\eta_{act} = a \ln(i) + b \quad (22)$$

With:

$$a = \frac{RT}{\alpha nF} \quad (23)$$

$$b = -\frac{RT}{\alpha nF} \ln(i_0) \quad (24)$$

The coefficients a and b are function of temperature, they are calculated in an empirical way at each temperature.

Concentration overvoltage

In limiting performance of stack the concentration overvoltage appears in form [6] [8]:

$$\eta_{con} = \frac{RT}{nF} \ln\left(1 - \frac{i}{i_L}\right) \quad (25)$$

Where:

i_L : Limiting current ($i_L=45A$)

Thermal modelling

A SOFC is submitted to three fundamental heat transfers (conduction, convection and radiation). The heat transfer by radiation is neglected in this article. The species transportation and electrochemical effects are also considered. In order to make the model easy to solve, a model 2D by nodal network of one cell is developed.

Figure 6 shows a 2D nodal network representation of the studied cell. This last is composed with seven isothermal control volumes, all represented with a temperature node. It permits to consider heat transfers by convection and conduction and by the mass transportations as well through the conserved volumes. The volumes are the electrolyte between the anode and cathode channels, the fluid channels (air, H₂) and the anodic and cathodic interconnects.

The three kinds of heat and mass transfers which are taken into account are gathered in table 3 with the specific equivalent thermal resistances. Then, knowing these expressions, each heat and mass transfer can be written as an expression of the difference of temperature between two nodes and the thermal resistance [9] [10] [11].

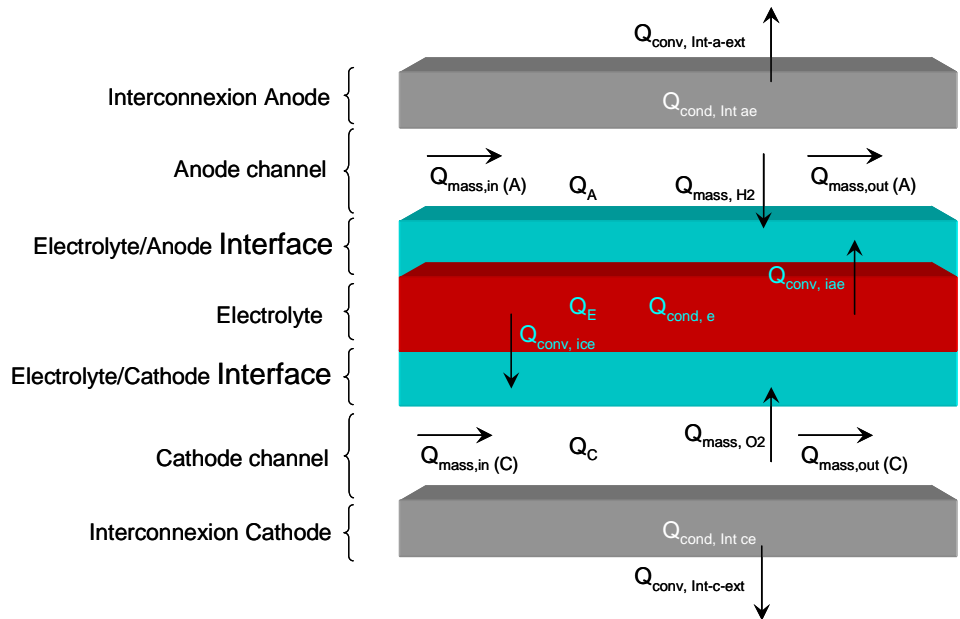


Figure 6 Heat transfer in cell SOFC

Heat flux	Heat flow (W) and heat resistance (K.W ⁻¹)
Heat transfer by conduction heat between T ₁ and T ₂	$\phi = \frac{\lambda S}{e} (T_1 - T_2)$ λ : Thermal conductivity (W.m ⁻¹ .K ⁻¹) S : Heat transfer area (m ²) e : Length (m) $R_{th} = \frac{e}{\lambda S}$
Heat transfer by convection heat	$\phi = hS(T_1 - T_2)$ h : Heat convection coefficient (W.m ² .K ⁻¹) $R_{th} = \frac{1}{hS}$
Heat and mass fluxes	$\phi = \dot{m} c (T_1 - T_2)$ \dot{m} : mass flow of gas (kg.s ⁻¹) c : mass specific heat at to constant pressure (J.kg ⁻¹ .K ⁻¹) $R_{th} = \frac{1}{\dot{m} c}$

Table 3 Calculation of the heat flow and the heat resistance

Thermal model of one cell

The modelling of the transient thermal state of the cell is also realized thanks to the nodal network shown in figure 7. Heat capacity at particular nodes (for which the thermal inertia is not neglected) gives the transient duration of the modelling.

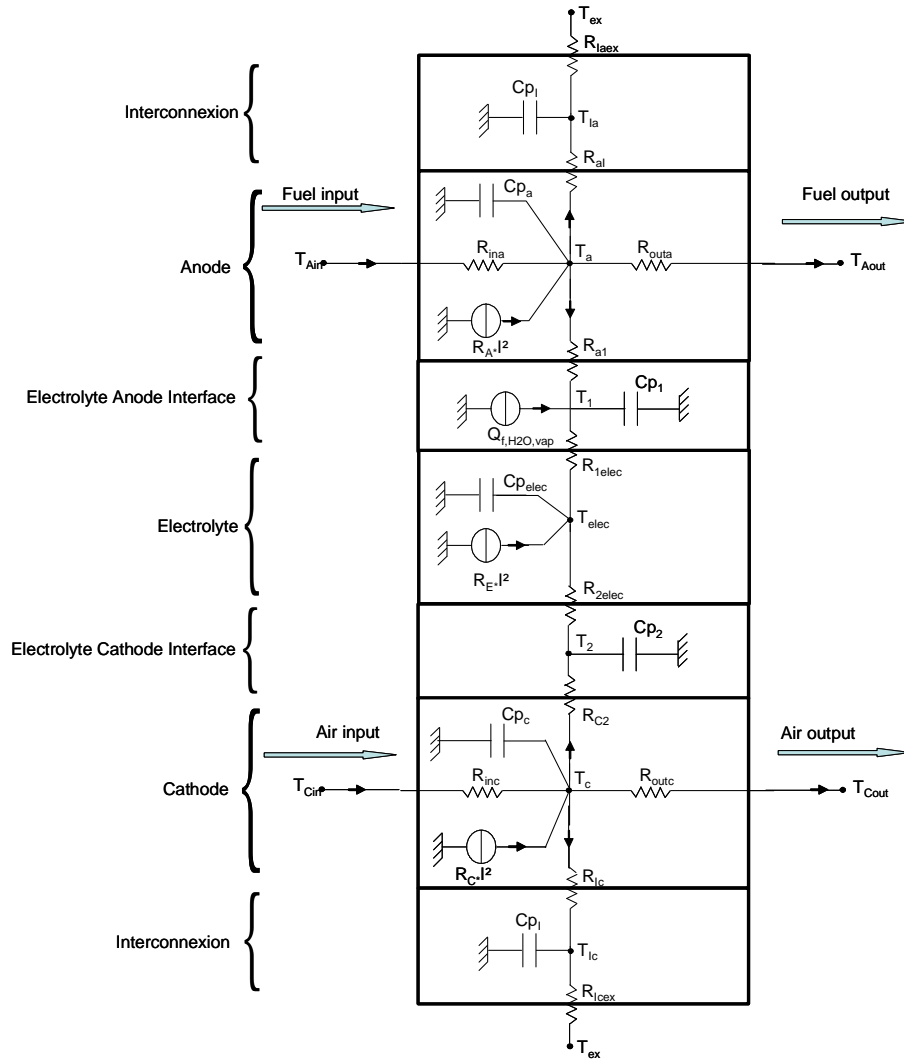


Figure 7 Cell thermal modelling

The thermal energy balance issued from the first thermodynamic law is then computed at each node of the network. It permits to obtain a transient analytical equation for each node. Then, the system of equations is expressed as a matrix system easily solved. We obtain, at the anode interconnexion:

$$\frac{(T_{la} - T_{ex})}{R_{laex_Cond} + R_{laex_Conv}} + \frac{(T_{la} - T_A)}{R_{al_Cond} + R_{al_Conv}} + Cp_{la} \frac{dT_{la}}{dt} = 0 \quad (26)$$

At the anode:

$$\frac{(T_A - T_{la})}{R_{al_Cond} + R_{al_Conv}} + \frac{(T_A - T_1)}{R_{a1}} + \frac{(T_A - T_{Air})}{R_{ina}} + \frac{(T_A - T_{Aout})}{R_{outa}} + Cp_a \frac{dT_A}{dt} = R_A \times I^2 \quad (27)$$

For the Electrolyte Anode Interface:

$$\frac{(T_1 - T_A)}{R_{a1}} + \frac{(T_1 - T_{elec})}{R_{1elec_Cond} + R_{1elec_Conv}} + Cp_{ea} \frac{dT_1}{dt} = Q_{f,H2O,vap} \quad (28)$$

Concerning the electrolyte:

$$\frac{(T_{elec} - T_1)}{R_{1elec_Cond} + R_{1elec_Conv}} + \frac{(T_{elec} - T_2)}{R_{2elec_Cond} + R_{2elec_Conv}} + Cp_{elec} \frac{dT_{elec}}{dt} = R_E \times I^2 \quad (29)$$

At the Electrolyte Cathode Interface:

$$\frac{(T_2 - T_{elec})}{R_{2elec_Cond} + R_{2elec_Conv}} + \frac{(T_2 - T_C)}{R_{C2}} + Cp_{ec} \frac{dT_2}{dt} = \quad (30)$$

For the cathode:

$$\frac{(T_C - T_2)}{R_{C2}} + \frac{(T_C - T_{Ic})}{R_{Ic_Cond} + R_{Ic_Conv}} + \frac{(T_C - T_{Cin})}{R_{inC}} + \frac{(T_C - T_{Cout})}{R_{outC}} + Cp_c \frac{dT_c}{dt} = R_C \times I^2 \quad (31)$$

Finally, for the cathode Interconnexion:

$$\frac{(T_{Ic} - T_C)}{R_{Icex_Cond} + R_{Icex_Conv}} + \frac{(T_{Ic} - T_{ex})}{R_{Ic_ond} + R_{Ic_Conv}} + Cp_{Ic} \frac{dT_{Ic}}{dt} = 0 \quad (32)$$

The system equations (26-32) can be written with matrix and vector expressions:

$$[G] \cdot [T] + [Cp_i] \cdot \left[\frac{dT}{dt} \right] = [Q_i] \quad (33)$$

Where:

$$[T] = [T_{Ia} \quad T_a \quad T_1 \quad T_{elec} \quad T_2 \quad T_c \quad T_{Ic}]^T \quad (34)$$

$$G = \begin{bmatrix} G_{11} & G_{12} & 0 & 0 & 0 & 0 & 0 \\ G_{21} & G_{22} & G_{23} & 0 & 0 & 0 & 0 \\ 0 & G_{32} & G_{33} & G_{34} & 0 & 0 & 0 \\ 0 & 0 & G_{43} & G_{44} & G_{45} & 0 & 0 \\ 0 & 0 & 0 & G_{54} & G_{55} & G_{56} & 0 \\ 0 & 0 & 0 & 0 & G_{65} & G_{66} & G_{67} \\ 0 & 0 & 0 & 0 & 0 & G_{76} & G_{77} \end{bmatrix} \quad (35)$$

$$G_{ij} = G_{ji} \quad (36)$$

Table 3 illustrates the conductance G_{ij} used in matrix (35):

G_{11}	$\frac{1}{R_{Iaex_cond} + R_{Iaex_conv}} + \frac{1}{R_{al_cond} + R_{al_conv}}$
$G_{12} = G_{21}$	$\frac{-1}{R_{Iaex_cond} + R_{Iaex_conv}}$
G_{22}	$\frac{1}{R_{al_cond} + R_{al_conv}} + \frac{1}{R_{a1}} + \frac{1}{R_{ina}} + \frac{1}{R_{outa}}$
$G_{23} = G_{32}$	$\frac{-1}{R_{a1}}$
G_{33}	$\frac{1}{R_{a1}} + \frac{1}{R_{Ielec_cond} + R_{Ielec_conv}}$
$G_{34} = G_{43}$	$\frac{-1}{R_{Ielec_cond} + R_{Ielec_conv}}$

G_{44}	$\frac{1}{R_{1elec_cond} + R_{1elec_conv}} + \frac{1}{R_{2elec_cond} + R_{2elec_conv}}$
$G_{45} = G_{54}$	$\frac{-1}{R_{2elec_cond} + R_{2elec_conv}}$
G_{55}	$\frac{1}{R_{2elec_cond} + R_{2elec_conv}} + \frac{1}{R_{C2}}$
$G_{56} = G_{65}$	$\frac{-1}{R_{C2}}$
G_{66}	$\frac{1}{R_{C2}} + \frac{1}{R_{IC_cond} + R_{IC_conv}} + \frac{1}{R_{inC}} + \frac{1}{R_{outC}}$
$G_{67} = G_{76}$	$\frac{-1}{R_{IC_cond} + R_{IC_conv}}$
G_{77}	$\frac{-1}{R_{Icex_cond} + R_{Icex_conv}} + \frac{1}{R_{Ic_cond} + R_{Ic_conv}}$

Table 3 Calculation of the conductance

The matrix $[Cp_i]$ of the heat capacities is a diagonal matrix expressed with relation (37).

$$[Cp_i] = \begin{bmatrix} Cp_I & 0 & 0 & 0 & 0 & 0 & 0 \\ 0 & Cp_a & 0 & 0 & 0 & 0 & 0 \\ 0 & 0 & Cp_1 & 0 & 0 & 0 & 0 \\ 0 & 0 & 0 & Cp_{elec} & 0 & 0 & 0 \\ 0 & 0 & 0 & 0 & Cp_2 & 0 & 0 \\ 0 & 0 & 0 & 0 & 0 & Cp_c & 0 \\ 0 & 0 & 0 & 0 & 0 & 0 & Cp_I \end{bmatrix} \quad (37)$$

$[Q_i]$ is the vector of internal power generation.

$$[Q_i] = \begin{bmatrix} \frac{T_{ex}}{R_{Iaex_cond} + R_{Iaex_conv}} \\ \frac{T_{ina}}{R_{ina}} + \frac{T_{outa}}{R_{outa}} + R_A \times I^2 \\ Q_{f,H2O,vap} \\ R_E \times I^2 \\ 0 \\ \frac{T_{inC}}{R_{inC}} + \frac{T_{outC}}{R_{out2}} + R_C \times I^2 \\ T_{ex} \\ \frac{T_{ex}}{R_{Icex_cond} + R_{Icex_conv}} \end{bmatrix} \quad (38)$$

Where:

R_A : The anode resistance

R_C : The cathode resistance

R_E : The electrolyte resistance

$Q_{f,H_2O,vap}$: The water formation energy at anode side, is given by flowing relation:

$$Q_{f,H_2O,vap} = F_{con,H_2} \times \Delta H_{f,H_2O} \quad (39)$$

Results and discussion

The three models (fluidic, thermal and electric) are coupled. Simulation at constant current is performed. Thermal dynamic effect is heat capacity.

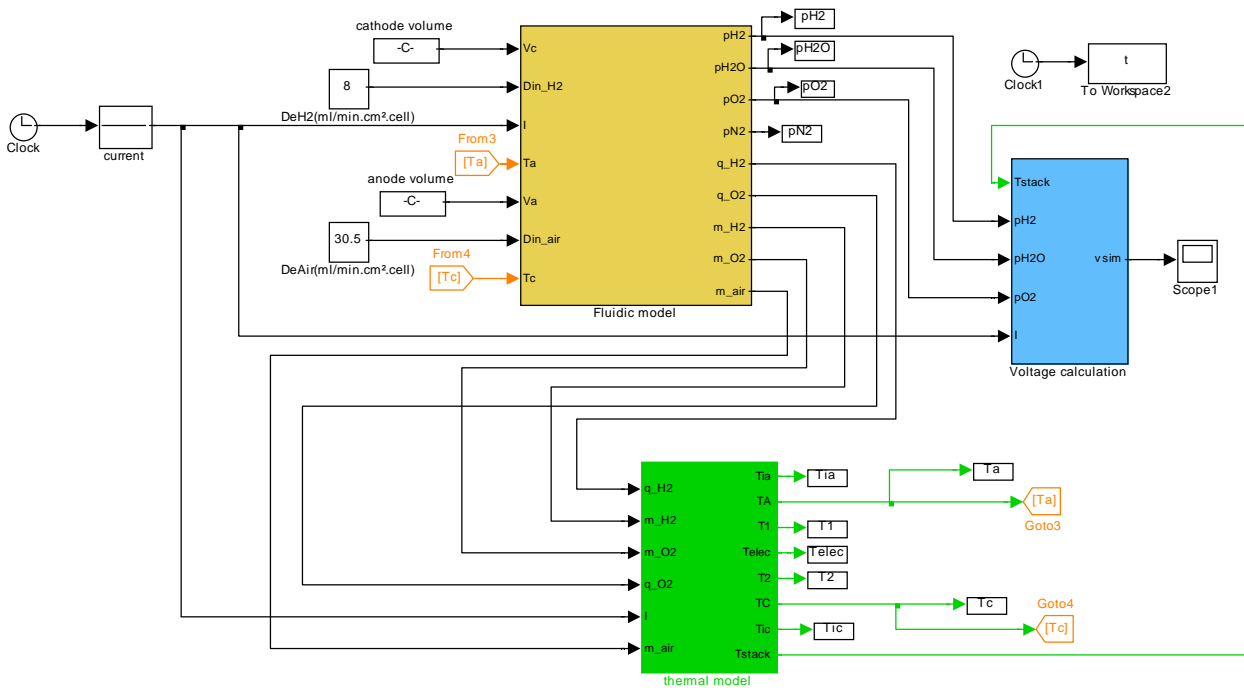


Figure 8 The complete model developed with Matlab Simulink

Experiments have been performed at three temperatures of the ambient air in the furnace: a low operating temperature (700°C), high operating temperature (800°C) and nominal operating temperature (750°C). For all temperatures, the inlet mass flow in anode and cathode are taken constant ($D_{H_2} = 8 \text{ ml} / \text{min.cm}^2.\text{cell}$, $D_{air} = 30.5 \text{ ml} / \text{min.cm}^2.\text{cell}$).

In the model, the temperature of the cathode is very close to the temperature of the furnace, because the conduction and convection between the interconnect and the cathode are low. So, these two temperatures are taken equal in the simulation.

Figure 9,10 and 11 show the polarization and power curves. At average current range where the ohmic drop is dominating, the model follows exactly the experimental results. At low current, where activation overvoltages are dominating, a light difference can be noticed between the model and the experimental because of the low acquisition frequency of the test bench which does not give enough points at low current.

At 800°C, concentration overvoltage has a noticeable contribution to the voltage drop at high current. A 700°C and 750°C, experimental results aren't available because tests haven't been performed for stack safety reasons.

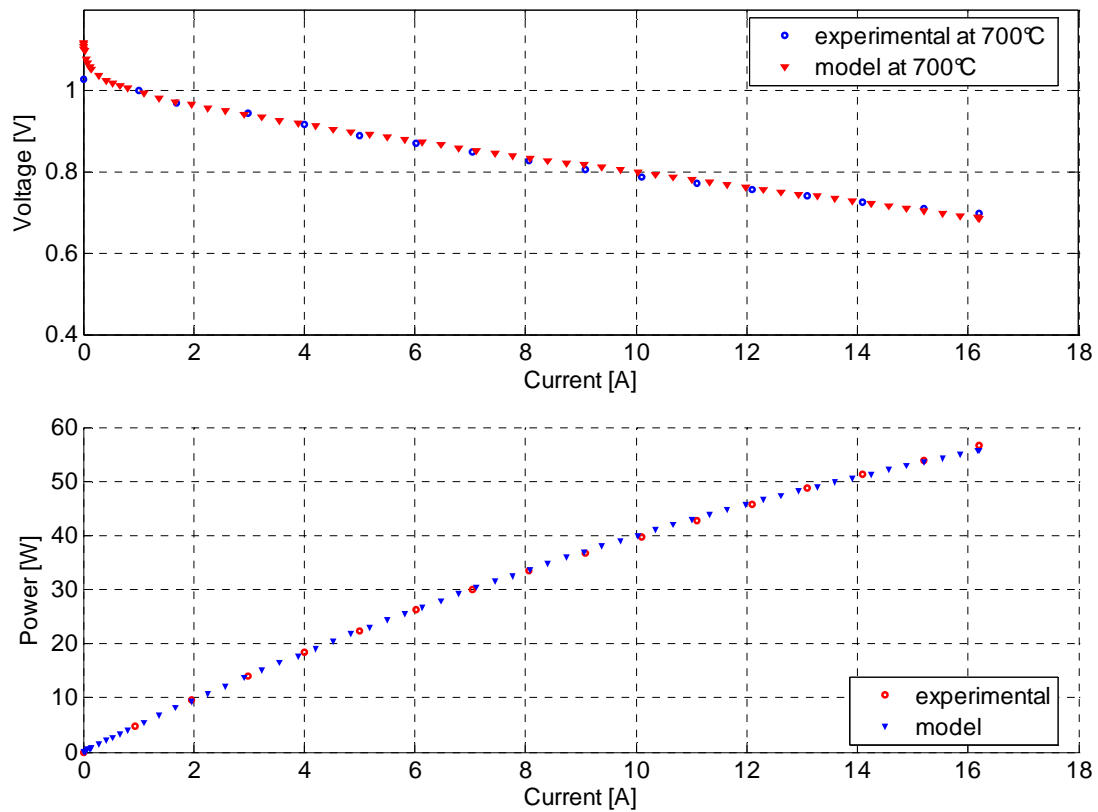


Figure 9 Polarization and power curves at 700°C

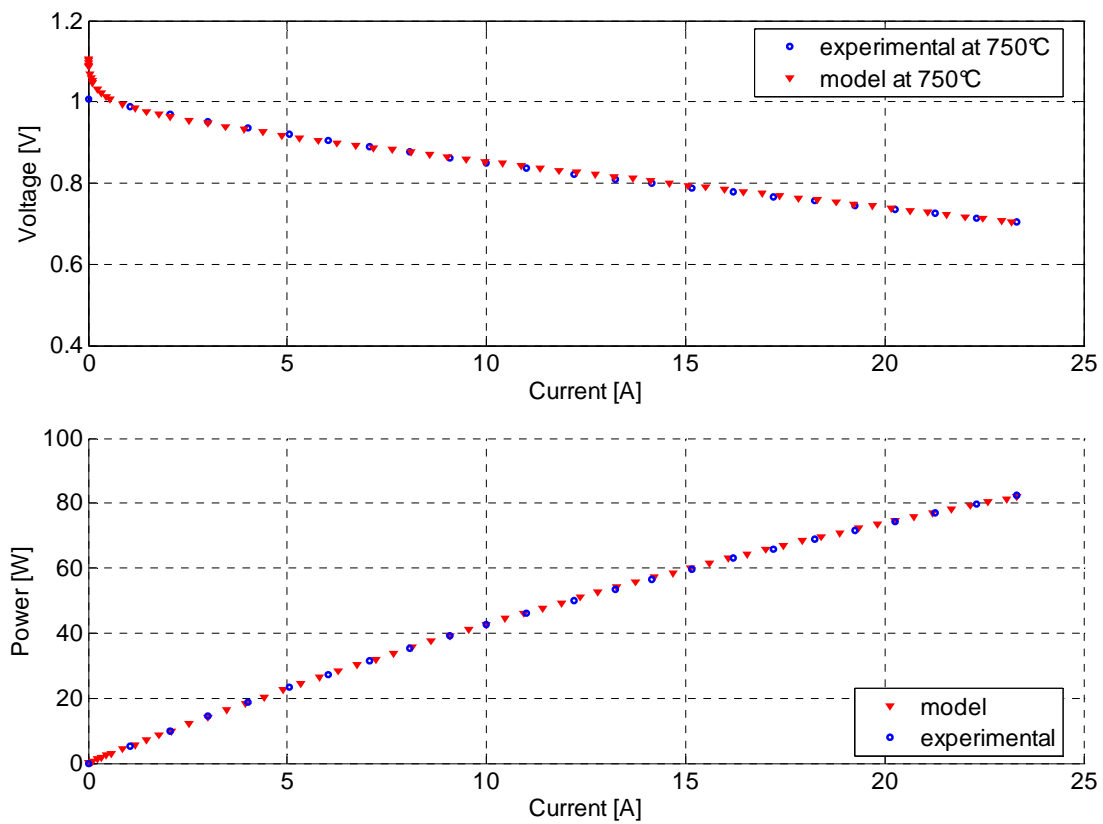


Figure 10 Polarization and power curves at 750°C

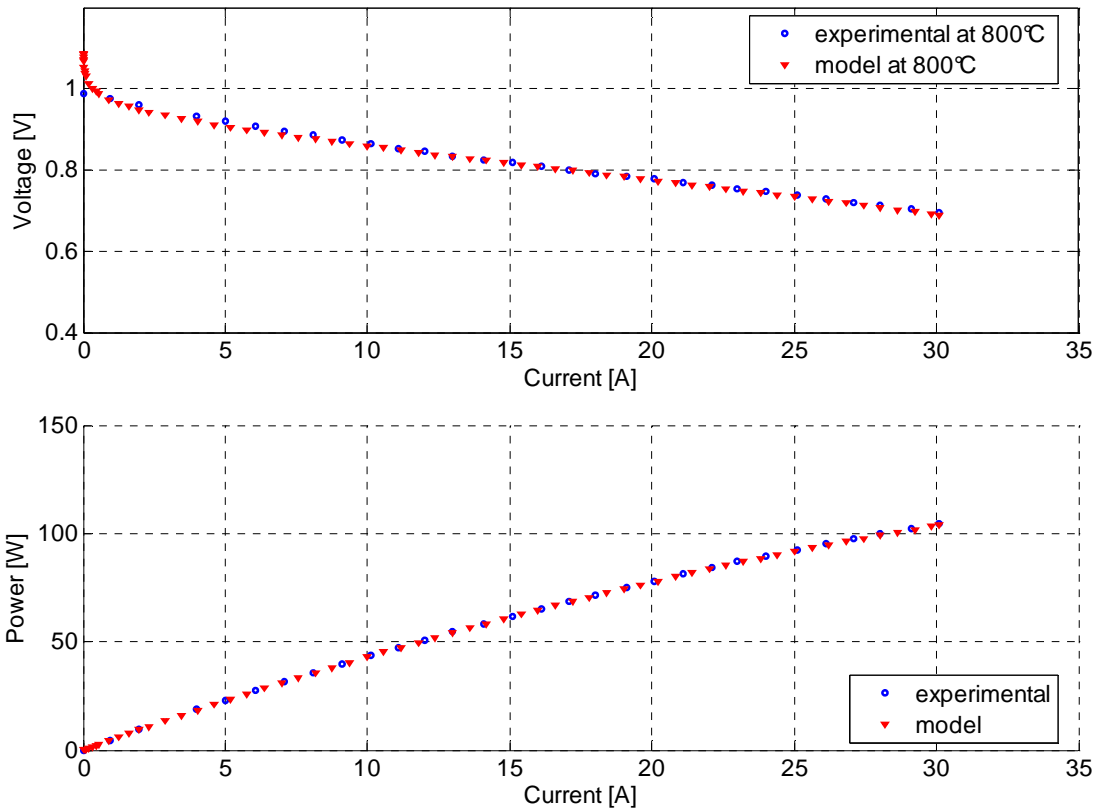


Figure 11 Polarization and power curves at 800°C

To observe the effect of the temperature on the stack voltage, the figure 12 shows the three polarization curves.

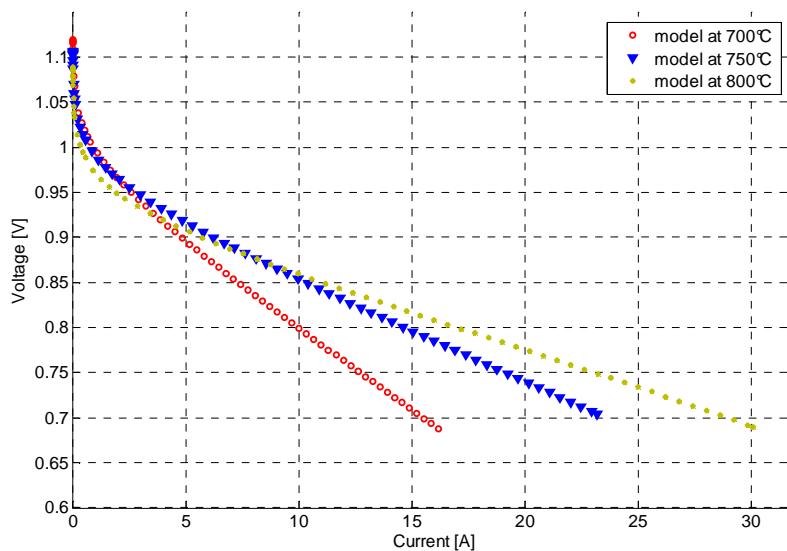


Figure 12 Polarization curve

In order to compare the partial pressures of the chemical species in the anode and cathode side, figure 14 shows the partial pressures of chemical species at 700°C.

On the anode side, the water formation reaction increases the partial pressure of water and the reduction of the hydrogen mole number due to the reaction (1) in the Anode/electrolyte Interface causes a reduction of the hydrogen partial pressure.

In the cathode side, the oxygen is consumed in the chemical reaction (2) which justifies the diminution of the oxygen partial pressure in the cathodic compartment and the nitrogen is not consumed in cathode side, so its partial pressure increases.

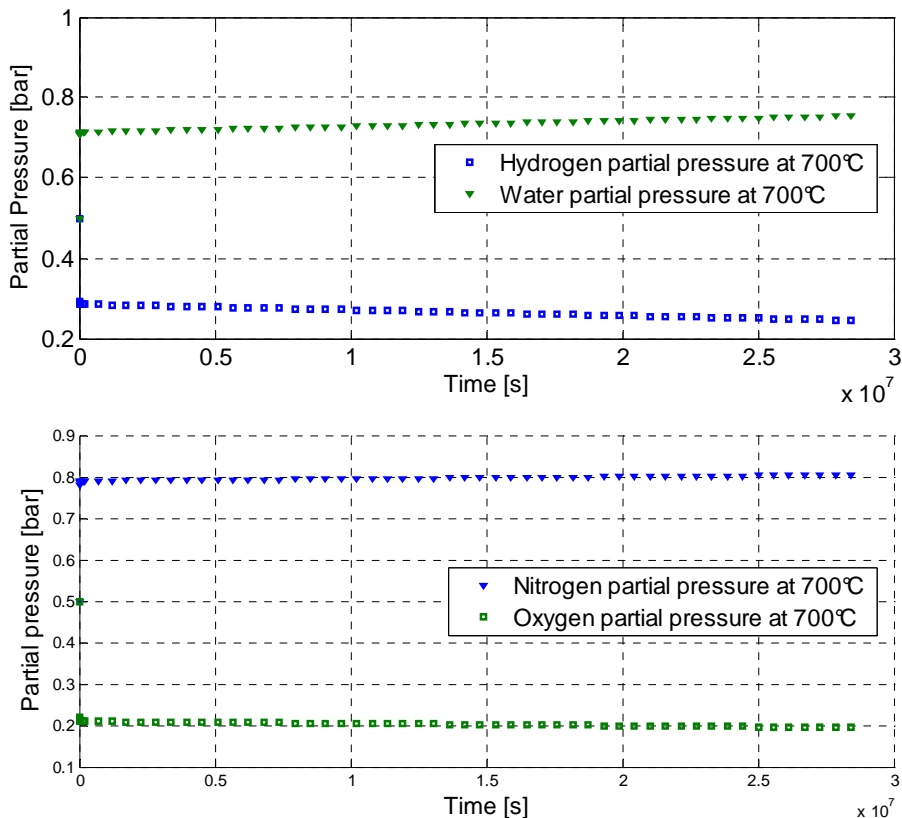


Figure 13 Species partial pressure at 700°C

At high temperature, the heat transfer between the solid parts and fluid (air or hydrogen) of the cell becomes important. The figure 15 shows the anode and cathode temperature simulation with null current and another with not null current.

The anode and cathode have the same time-constant because they have the same heat capacity and the same volume.

The temperature of the anode and cathode are close with null current because there is no convection exchange between electrolyte and electrodes due to the absence of the O^{2-} migration in the electrolyte.

With not null current, the temperature of the anode becomes higher than the temperature of cathode due to the energy of water formation in the Anode/Electrolyte Interface and also the ohmic energy ($R_A \cdot I^2$).

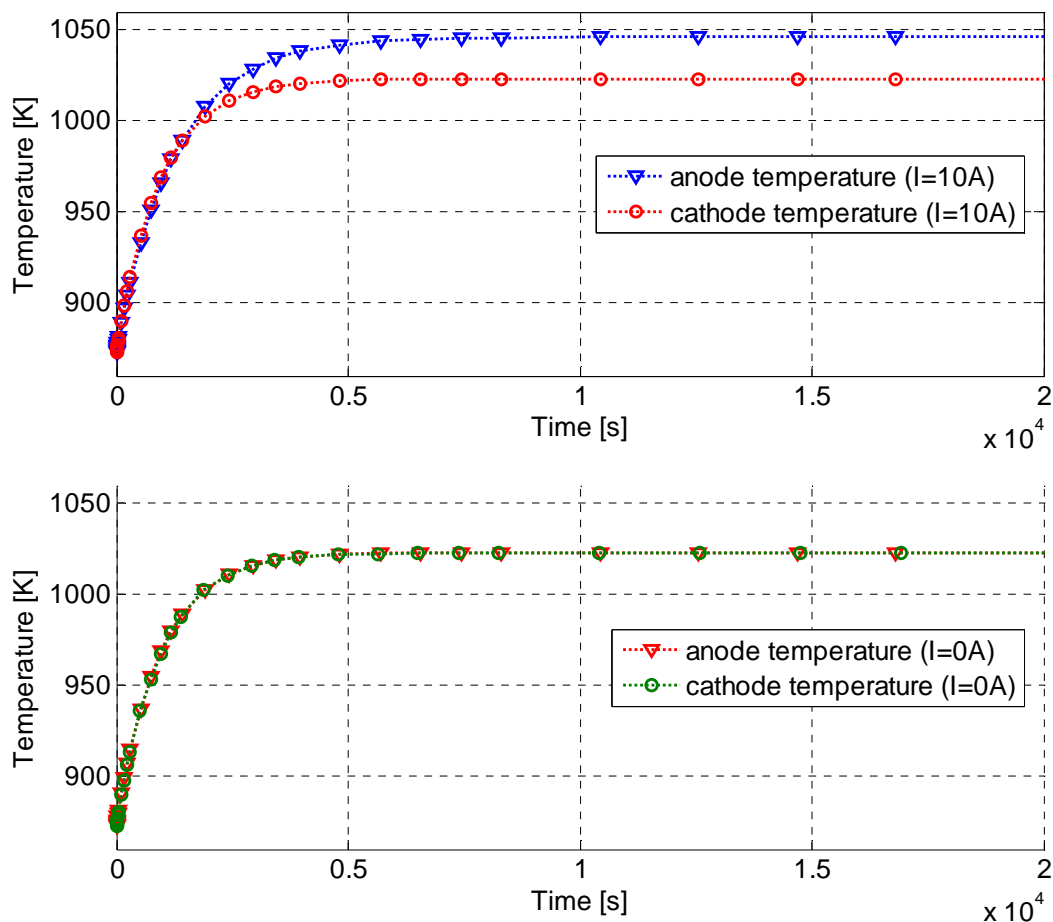


Figure 14 Anode and cathode temperature

Conclusion

In this paper, a simulation of a SOFC combining thermal, fluid and electrical models is developed to study its steady-state and thermal transient behaviour. The thermal model is based on nodal network with seven nodes in each cell. The energy balances in each node are taken and solved by Matlab Simulink. In this model, conduction, convection heat, species transportation and electrochemical effects are taken into account.

The fluid model is based in electric fluid analogy. The electric model is based in Nernst equation, Ohmic, activation and concentration overvoltages.

Experimental results on the 5 cell stack have been supplied by the HTceramix company for validation.

In the future, the radiation effect will be also considered and the electrical transient as well.

Acknowledgments

I am indebted to the people who have provided assistance, encouragement in L2ES laboratory. To HTceramix company, for its support, guidance and good collaboration.

Financial support for this work and my thesis was provided partly by Belfort general council and partly by European FELICITAS project (in which I am partner, and work in the PEFC and SOFC coupling).

References

- [1] Moussa Chnani, Hattab Maker, Denis Candusso, Marie-Cécile Péra and Daniel Hissel, Electrical Analogy Modelling of PEFC System Fed by a Compressor, Lucerne, Switzerland, July 2005
- [2] Kouros Sedghisigarchi, Ali Feliachi, Dynamic and Transient Analysis of Power Distribution Systems With Fuel Cells-Part I: Fuel- Cell Dynamic Model, IEEE Transactions on Energy Conversion, vol. 19, No. 2, June 2004
- [3] J. Padullés, G.W. Ault, J.R. McDonald, An integrated SOFC plant dynamic model for power systems simulation, Journal of Power Sources 86 (2000) 495-500, October 1999
- [4] S. Companari, P. Iora, Definition and sensitivity analysis of finite volume SOFC model for a tubular cell geometry, Journal of Power Sources 132 (2004) 113-126, January 2004
- [5] Yutong Qi, Biao Huang, Karl T. Chuang, Dynamic modelling of solid oxide fuel cell: The effect of diffusion and inherent impedance, Journal of Power Sources, vol 150, pages 32-47, 4 October 2005
- [6] Subhash C Singhal and Kevin Kendall, High Temperature Solid Oxide Fuel Cells Fundamentals, Design and Applications, Elsevier Advanced Technology
- [7] Paola Castamagna, Azra Selimovic, Marc Del Borghi, Gerry Agnew, Electrochemical model of integrated planar solid oxide fuel cell (IP-SOFC), Journal of Power Sources 102 (2004) 61-69, February 2004
- [8] D.A. Noren, M.A. Hoffman, Clarifying the Butler–Volmer equation and related approximations for calculating activation losses in solid oxide fuel cell models, Journal of Power Sources, vol 152, pages 175-181, 1 December 2005
- [9] K. Sudprasert, R.P Travis and R.F Martinez-Bots, A computational fluid dynamic model of a solid oxide fuel cell, Imperial college of London, Department of Mechanical Engineering, London UK, Proc. IMechE Vol. 219 Part A: J. Power and Energy, . IMechE 2005
- [10] X. Xue, J. Tang, N. Sammes, Y. Du, Dynamic modeling of single tubular SOFC combining heat/mass transfer and electrochemical reaction effects, Journal of Power Sources 142 (2005) 211-222, November 2004
- [11] David J. Hall, R. Gerald Colclaser, Transient modelling and simulation of tubular solid oxide fuel cell, IEEE Transactions on Energy Conversion, vol. 14, No. 3, September 1999